DOI: 10.61782/fa.2025.0131

FORUM ACUSTICUM EURONOISE 2025

ANALYSIS OF DEFECTS IN ROLLING BEARINGS USING VIBROACOUSTIC AND ULTRASONIC TECHNIQUES

Emanuele Voltolini [1] **Mirko Monaco**[1] **Enrico Armelloni**[1]
Marco Cocconcelli[3] **Andrea Toscani**[2] **Fabio Immovilli**[3] **Elisabetta Manconi**[*1]
[1] Department of Engineering for Industrial Systems and Technologies, University of Parma, Italy
[2] Department of Engineering and Architecture, University of Parma, Italy
[3] Department of Engineering Science and Methods, University of Modena and Reggio Emilia, Italy

ABSTRACT

This study explores the comparative effectiveness of microphones (standard and ultrasonic) and accelerometers in detecting defects in bearings. Defects in rolling bearings generate acoustic waves with a rich content in high frequencies. Both accelerometer and microphone data allow for Envelope Analysis or Amplitude Demodulation (low frequency), while only ultrasonic microphone data enable high-frequency analysis. The study investigates the advantages of using non-contact microphones to capture this high-frequency content easily. The non-contact nature of microphones also eliminates the risk of altering the machine's operational conditions, ensuring easy and secure data collection. Various bearings with different defects were investigated by conducting controlled experiments on a test bench. The analysis was carried out by exploiting statistical indicators, e.g., Kurtosis, Crest Factor, Impulse Factor, etc., and energy-based analysis techniques to compare low- and high-frequency results. Results of the different analyses were presented and discussed, showing the potential use of mixed accelerometric, acoustic, and ultrasonic measurements for practical predictive maintenance of rotating machines.

Keywords: *bearings, predictive maintenance, ultrasound microphone, microphone, accelerometer.*

[*]***Corresponding author***: elisabetta.manconi@unipr.it

1. INTRODUCTION

In recent years, predictive maintenance has become increasingly important in industry due to its ability to predict failures and reduce downtime [1-3]. Vibration analysis, primarily based on the use of accelerometers, is one of the most established techniques for monitoring the condition of rotating machinery [4]. In fact, it can provide accurate and repeatable data for condition monitoring of industrial machines, and it is a well-developed and thoroughly studied technique. However, accelerometers need to be installed on the machine in close proximity to the component being analyzed [5-7]. This can pose a challenge since there are practical situations where the sensors cannot be mounted properly or may interfere with the machine's structure. In more severe cases, they might not be installable close to the area that needs monitoring, or, even more critically, they cannot be utilized at all, such as for safety concerns. Compared to acceleration analysis, acoustic analysis using microphones offers several advantages, including the ability to detect signals at higher frequencies than traditional accelerometers and the capability to monitor machines without direct contact. In this context, this paper investigates the use of microphones, particularly ultrasonic microphones, in addition to accelerometers for monitoring the condition of mechanical components, particularly rolling bearings [8]. In addition, the combined use of vibration and acoustic signals could improve the accuracy of early fault detection, allowing more timely and efficient maintenance intervention. The paper focuses on the analysis of the energy content in the acoustic signal and the use of statistical indicators, without going into details of advanced spectral processing or machine learning techniques. The aim is to assess the effectiveness of an approach based on simple, yet meaningful, metrics that complement traditional predictive maintenance methods, enhance early failure detection, and to evaluate the effectiveness of the hybrid accelerometric-microphonic approach applied to these techniques.

2. ANALYSIS PARAMETERS

This study uses low-complexity signal analysis parameters to assess their applicability in industrial predictive maintenance [9-10].
Kurtosis is here applied as a key indicator. It measures the deviation from the mean and reflects the presence of sharp peaks or heavy tails in a signal. Statistically, it is defined as the fourth standardized moment:

$$Kurtosis = E\left[\left(\frac{X-\mu}{\sigma}\right)^4\right] = \frac{\mu_4}{\sigma^4}$$
$$\frac{\mu_4}{\sigma^4} = \frac{\frac{1}{N}\sum_{i=1}^{N}(x(i)-\mu)^4}{\left(\frac{1}{N}\sum_{i=1}^{N}(x(i)-\mu)^2\right)^2} \tag{1}$$

A normal distribution of data presents a kurtosis equal to 3, and distributions with a kurtosis greater than that value are defined as leptokurtic. Leptokurtic distributions present thicker tails, i.e. have more data far from the mean value; typically, vibrations produced by defects in rolling bearings show Leptokurtic behavior.
The second indicator used is the RMS (Root Mean Square), defined as:

$$RMS = \sqrt{\frac{1}{N}\sum_{i=0}^{N}\left(x^2(i)\right)} \tag{2}$$

The RMS value of vibrations produced by a damaged bearing is sensibly greater than a healthy bearing one.
Some impulsive metrics indicators, such as the crest factor and the impulse factor were used to evaluate the peak component of the signal. Crest factor is defined as the peak value divided by the RMS value:

$$Crest\ Factor = \frac{|x_{peak}|}{\sqrt{\frac{1}{N}\sum_{i=0}^{N}\left(x^2(i)\right)}} \tag{3}$$

The impulse factor is defined as the ratio of the peak value to the arithmetic mean of the absolute values of the signal:

$$Impulse\ Factor = \frac{|x_{peak}|}{\frac{1}{N}\sum_{i=0}^{N}|x(i)|} \tag{4}$$

Impulsive metrics are important in bearings fault analysis because the formation and growth of defects cause impulsive forces to be generated during bearing operation.

To conclude, spectral energy was used to represent the energy contained in the various third octave frequency bands. Spectral energy is defined as the sum of the squared absolute value of the Fourier-transformed signal:

$$E(f) = \sum |X(f)|^2 \tag{6}$$

According to Percival's theorem, the spectral energy calculated over the whole spectrum is equal to the overall signal energy. In this study, particular attention was paid to the relationship between the spectral energies calculated from the signals of damaged bearings to those from healthy bearings for each data acquisition batch.

3. METHODOLOGY

3.1 Data Acquisition

Several data acquisitions were conducted by varying both fault type and bearing operating condition. This section details the equipment and sensors used, including their technical specifications. In addition, a brief overview of the test environments and experimental settings are provided. All the measurements were carried out at the laboratories of the University of Modena and Reggio Emilia.

3.1.1 Sensors and data acquisition devices

The same data acquisition systems were used in the tests to ensure consistency and comparability of results. The whole system is composed of a data acquisition system, one measurement microphone, one ultrasound microphone and one accelerometer. The ZoTech[1] Data Acquisition System (DAQ) was used to record the microphone and accelerometer signals, composed of a Sensor Network Interface (DIN0264) and a Sensor Acquisition Node (AIN0824). This architecture makes use of a digital bus implemented on an Unshielded Twisted Pair to connect one or more AIN0824 boards to a data storage system (e.g., a laptop or an industrial PC) using a DIN0264 board. The implementation of a digital communication guarantees perfect synchronization between the acquired signals, both in term of jitter and latency [9-10] making it a perfect system for acquiring many transducers with time synchronization, mandatory for the computation of the most advanced diagnostic metrics [11-12]. The system operates at a sampling rate of 48 kHz with a resolution of 24 bits, ensuring accurate signal representation. A full-scale range of ±5V was configured for both sensors to optimize

[1] www.zotech.it/en

dynamic range and measurement fidelity. Further specifications are given in Tab. 1.

Table 1. ZoTech data acquisition system

Specification	Value
Number of inputs	64
Sampling Rate	48 kHz
Resolution	24 bits
Connection	USB 2.0

The Ultramic 384K WIND ultrasonic microphone (Tab. 2) has a built-in recording system with a sampling rate of 384 kHz and a resolution of 16 bits. This configuration allows accurate acquisition of ultrasonic signals up to 192 kHz, effectively covering the entire operating range of the microphone, which is critical for detecting high-frequency fault signatures.

Table 2. Ultrasound Microphone Ultramic 384K WIND (Dodotronic), technical data.

Specification	Value
Frequency Range	1 to 100 kHz
Sampling Rate	384 kHz
Resolution	16 bits
Connection	USB 2.0

For vibration measurements, the Piezotronics 603M170 PCB sensor was used (Table 3), which offers a frequency range up to 14 kHz and a sensitivity of 100 mV/g over one axis (mono-axial). This ensures the detection of mechanical vibrations in the typical range of failure frequencies.

Table 3. Accelerometer PCB Piezotronics 603M170, technical data.

Specification	Value
Sensitivity (±10%)	100 mV/g
Measurement Range	±80g
Frequency Range	0.4 Hz to 14 kHz

The Brüel & Kjær 4189 omnidirectional microphone was used as the acoustic transducer (Table 4), which offers a flat frequency response from 6 Hz to 20 kHz with a sensitivity of 50 mV/Pa. Its wide and stable response range enables accurate capture of low-frequency and high-frequency acoustic emissions, facilitating a comprehensive analysis of how potential damage affects the entire acoustic spectrum.

Table 4. Microphone and Preamplifier Bruel&Kjaer 4189-1706, technical data.

Specification	Value
Diameter	½inch
Sensitivity	50 mV/Pa
Frequency Range	6.3 Hz to 20 kHz

3.1.2 First test condition

In Fig. 1(a), a schematic diagram illustrates the configuration of the first test condition. The system consists of a three-phase motor with a bearing mounted directly on the shaft. An accelerometer is placed over the bearing seat to capture vibrations in the radial direction.

The Ultramic 384K WIND is placed 20 cm in front of the bearing, directly aligned with it. The microphone is connected via USB 2.0 to a PC running Audacity software, which records the signal at 384 kHz.

The measurement microphone (Brüel & Kjær 4189) is placed 45 cm from the bearing to capture the machine's overall acoustic emissions. This microphone and accelerometer are connected to the ZoTech data acquisition system. Data from these sensors are recorded on a separate PC, as different interfaces are needed for different sampling rates.

The motor speed was set to 1000 rpm, and all test bearings were evaluated under this nominal operating condition. Measurements were conducted on a series of three SKF 6205 bearings, each subjected to different laboratory-induced wear conditions. The first bearing was new and served as a reference. The second bearing had damage to the outer ring induced by acid exposure, and the third was damaged by compression with a force greater than its rated load capacity. SKF 6205 bearing specifications are given in Tab. 5.

Table 5. SKF 6205 bearing specifications.

Specification	Value
Number of balls	9
Diameter of balls	7.94 mm
Pitch diameter	39.04 mm
Contact angle	0°

3.1.3 Second test condition

The second set of measurements, shown in Fig. 1.b, was conducted on a test bench specially designed for bearing analysis, the AV TEST BENCH, manufactured by AMC Vibro. This test bench consists of two three-phase asynchronous motors, one operating as a main motor and the other as a braking system, together with a gearbox

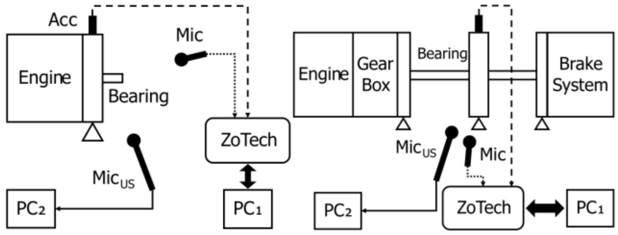

(a) (b)

Figure 1. (a) First test condition, (b) second test condition

(transmission rate 2,91:1) and a shaft supported by three rolling bearings. The test stand was used with a three-stage speed profile consisting of three constant-speed strokes at 1000-1500-2000 RPM measured on the motor side. The corresponding shaft speeds at which the bearing was tested were 343.64 RPM, 515.46 RPM and 687.29 RPM, due to the speed reduction of the gearbox. For these measurements, the accelerometer was mounted on the center bearing, and the two microphones were placed 15 cm in front of the bearing. The parameters of the data acquisition system remained unchanged from the previous test to ensure consistent measurement conditions. Measurements were conducted using two SKF YAR 204-2F bearings: the first bearing was healthy, with a minimum number of operating hours, while the second had a lab welding-induced damage on the outer ring. SKF YAR 204-bearing technical specifications are given in Tab. 6.

Table 6. SKF YAR 204 2F bearing specifications.

Specification	Value
Number of balls	8
Diameter of balls	7.938 mm
Pitch diameter	33.5 mm
Contact angle	0°

3.2 Data Processing

To ensure consistent and reliable statistical parameters for the detection of potential failures, the acquired signals were subjected to pre-processing, which included data slicing and filtering. Next, theoretical failure frequencies of the tested bearings were calculated based on their geometric parameters and rotational speed. Finally, envelope analysis and spectrogram visualization were performed to characterize the damage signatures of the defective bearings with respect to the healthy reference. The following subsections detail each step of the data processing workflow.

3.2.1 Pre-processing

In all test conditions, at least 1 minute of audio was recorded to ensure that the system reached a steady state condition. From each recording, 15 seconds of steady-state data are selected. In Fig. 2, an example of the raw, trimmed signal data from the three sensors is presented in both "healthy" and "damaged" conditions of the bearing. The data are then filtered with a Butterworth-type bandpass filter of order 5, matched to the characteristic frequency range of each sensor: for the accelerometer, the used filter range is 2 Hz to 14 kHz; for the microphone, the range is 6 Hz to 20 kHz and for the ultrasonic microphone goes from 1 to 100 kHz.

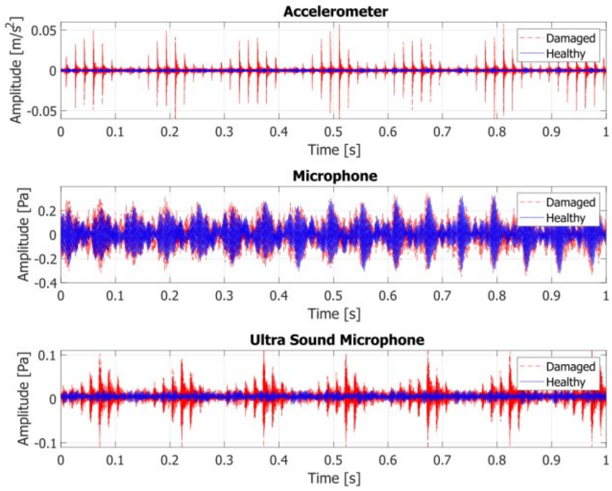

Figure 2. Time plot of 1 s for each sensor.

3.2.2 Calculus of bearings fault frequencies

To confirm and characterize the presence of defects manually induced on the bearings, characteristic failure frequencies were calculated based on bearing's geometric parameters and rotational speed, following the methodology described in [13]. These failure frequencies aid in identifying specific types of defects. The equations used are as follows:

$$f_{BPFO} = \frac{n}{2} f_r \left(1 - \frac{BD}{PD}\cos\beta\right) \tag{7}$$

$$f_{BPFI} = \frac{n}{2} f_r \left(1 + \frac{BD}{PD}\cos\beta\right) \tag{8}$$

$$f_{BFF} = \frac{PD}{BD} f_r \left[1 - \left(\frac{BD}{PD}\cos\beta\right)^2\right] \tag{9}$$

$$f_{FTF} = \frac{1}{2} f_r \left(1 - \frac{BD}{PD}\cos\beta\right) \tag{10}$$

where f_r is the shaft rotational frequency (in Hz), *BD* is the ball diameter and *PD* is the pitch diameter (distance between opposite rolling elements). The n parameter indicates the number of rolling elements and β is the contact angle of the rolling elements. The frequencies f_{BPFO}, f_{BPFI}, f_{BFF} , f_{FTF} are respectively: the Ball Pass Frequency Outer Race (characteristic of an outer ring fault), the Ball Pass Frequency Inner Race (for inner ring faults), the Ball Spin Frequency (related to rolling element defects), the Fundamental Train Frequency (associated with cage or retainer faults). The results are collected in Table 7.

Table 7. Bearings' fault frequencies with shaft speed respectively of 1000 and 343.64 rpm.

Parameters [Hz]	SKF 6205	SKF YAR204
Rotation Freq.	16.67	5.73
BPFO	59.75	20.53
BPFI	90.25	31.01
BFF	78.56	27.00
FTF	6.64	2.28

To confirm the presence of these defects in the recorded signals, Hilbert envelope analysis was applied to the accelerometer signal [13] to enhance the impulsive components caused by the bearing defects, making the defect-related frequencies more visible in the frequency domain. The Hilbert envelope spectrum, shown in Fig. 3, reveals the dominant spectral components associated with different types of damage. In the healthy bearing (black solid line), the spectrum is predominantly characterized by the shaft rotation frequency of 16.67 Hz and its harmonics, indicating normal operation. In contrast, for the first type of damage (dashed blue line), the spectrum has a distinct peak at the ball passage frequency on the outer raceway (BPFO) of 59.75 Hz, confirming the damage on the outer raceway. In addition, the presence of a peak at the train fundamental frequency (FTF) suggests a cage defect, while the side bands around the BPFO, spaced twice the FTF, indicating modulation effects due to the interaction between these fault components. For the second type of damage (dashed red line), the dominant peak at 78.6 Hz corresponds to the ball rotation frequency (BFF), while distinct peaks at the ball passage frequency within the stroke (BPFI), BPFO and FTF further confirm the presence of the multiple damages, induced by compression of the bearing.

3.2.3 Calculus of parameters in ⅓-octave band approach

To calculate statistical parameters for bearing defect detection, a preliminary analysis was performed on the entire spectrum of the pre-filtered signal.

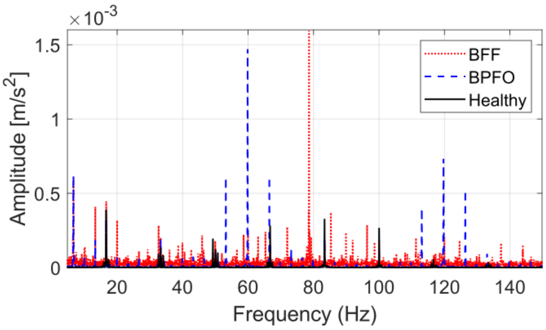

Figure 3. Spectrum of the Hilbert envelope of the accelerometer signal (SKF6205).

Subsequently, a ⅓-octave band approach was adopted to obtain a more in-depth view. This method was chosen because it offers an optimal compromise between frequency resolution and data manageability. Starting from the pre-processed signal (section 3.2.1), the data were segmented into one-third octave bands spanning the frequency range defined by the minimum and maximum central frequencies reported in Tab. 8. For each band, a 4th-order bandpass Butterworth filter was applied. The cutoff frequencies were calculated as:

$$f_{low} = \frac{f_c}{2^{1/6}} \;\; ; \;\; f_{high} = f_c \times 2^{1/6} \qquad (11)$$

where f_c is the central frequency of each band. Once the signal was filtered into its component ⅓ octave bands, the statistical parameters described in section **Errore. L'origine riferimento non è stata trovata.** were calculated for each band. These parameters provide insights into the signal's energy distribution and impulsiveness, which are critical in identifying the occurrence of bearing failures.

Table 8. 1/3 octave maximum and minimum central frequencies for all the sensors.

[kHz]	**Acc**	**Mic**	**UltraMic**
f_{c_min}	1	1	20
f_{c_max}	12.5	16	100

4. RESULTS AND DISCUSSION

This chapter presents the overall results of the two test conditions described in Sections 3.1.2 and 3.1.3, analyzed in terms of statistical parameters and spectral energy factor. Section 4.1 focuses on the first test condition, illustrating the results obtained for different types of damage at constant velocity. Section 4.2, on the other hand, examines the effects of a single type of damage at varying speeds.

4.1 Results at constant speed

The first testbed demonstrated promising results, showing clear distinctions in both statistical parameters and spectral energy analysis.

4.1.1 Statistical Parameter

Before calculating the parameters within one-third-octave bands, as shown in section 3, they were calculated over the entire spectrum. In Tab. 9, only the results for the ultrasonic microphone are presented because previous research has already validated the use of these statistical parameters with accelerometers. As is evident from the data, both types of bearing damage result in significant deviations from the "healthy" case, making these parameters an effective means of distinguishing between undamaged and damaged bearings. Fig. 4 shows the results obtained for the kurtosis for the three sensors, applying it to the one-third-octave bands as described in section 3.2.3. As expected, the accelerometer provided excellent results, particularly in the mid-to-high frequency ranges (3.5-5 kHz and 6-12 kHz), where the damage effects were most pronounced. The results obtained from the two microphones are also interesting, showing a significant increase in kurtosis at higher frequencies, particularly between 8 and 16 kHz. Although the difference between the "healthy" and the "damaged" cases is relatively small compared to the accelerometer results, it is noteworthy that despite being placed at a considerable distance from the bearing, the microphone still managed to detect the changes between the two conditions. The ultrasonic microphone, on the other hand, provided even sharper and more reliable results. It differentiated effectively between the two bearings, with damage to the outer ring (red bars) mainly affecting bands between 20 and 31.5 kHz. In the case of compression damage (ochre bars), the affected frequency range was from 20 to 63 kHz, with a peak at 40 kHz.

Table 9. Mean Statistical Parameters of different condition of the bearing, computed using ultrasonic microphone recordings.

	Healthy	**BPFO Damaged**	**BFF Damaged**
Kurtosis	2.4849	15.1926	11.1764
Impulse Factor	4.8443	19.7021	22.8560
Crest Factor	4.0316	12.0241	15.3572
RMS	0.0016	0.0105	0.0181

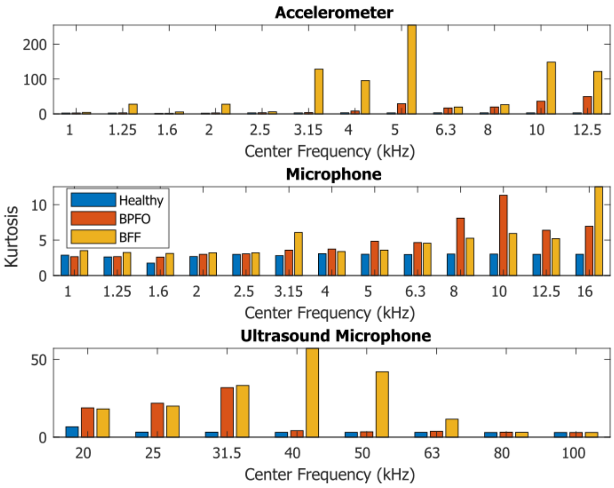

Figure 4. Kurtosis parameter in 1/3 octave bands representation, calculated for each sensor.

4.1.2 Spectral Energy Confrontation

Although spectral energy is not typically used as an absolute indicator of defects, the energy comparison between healthy and damaged bearings demonstrated significant results in this sense. As we did for the previous parameters, the spectral energy ratio was calculated in one-third octave bands to highlight the differences between damaged and healthy bearings. As shown in Fig. 5, the accelerometer reveals that the most significant energy differences between healthy and damaged bearings are concentrated in the mid- to high-frequency range, between 4 and 12.5 kHz, with a clear increase in spectral energy in the damaged cases. An interesting observation emerges from the analysis of the microphone measurement. In the case of compression damage, the increase in spectral energy is mainly in the low-mid frequencies, with a prominent peak at 1 kHz. In contrast, for outer ring damage, the frequencies affected are mainly in the upper-mid range, between 4 and 16 kHz, similar to what was observed with the accelerometer. For the ultrasonic microphone, the spectral energy increases significantly in the 20–40 kHz range, particularly in the compression-damaged bearing. The peak distribution differs with damage type: outer ring damage shows a dominant increase in the 20 kHz band, while compression damage peaks in the 35 kHz band.

4.2 Results at varying speed

This section presents the results referred to the second testbench, described in section 3.1.3. In Fig.6, we can observe the most statistically significant parameters (section

2) calculated over the entire signal spectrum at all three speeds tested.

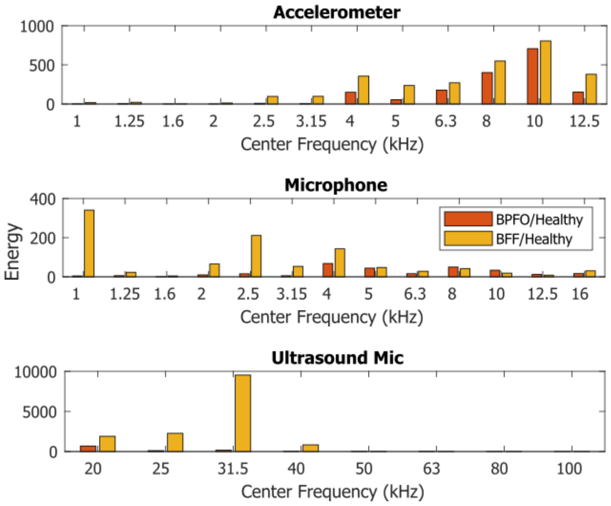

Figure 5. Spectral energy ratio between the damaged and healthy bearing signal, calculated for each sensor.

The first notable observation is that both the accelerometer and the ultrasonic microphone clearly distinguish between healthy and damaged bearings across all calculated parameters. Among these, impulse factor and kurtosis stand out as the most effective indicators. This demonstrates that full-band statistical analysis alone can reliably detect potential damage, regardless of shaft speed. In contrast, the standard microphone shows minimal variation across different speeds and conditions, indicating limited effectiveness over the entire frequency range. However, as shown in Fig. 7, when the analysis is narrowed to third-octave bands, this sensor also reveals useful information about fault presence. The plots illustrate only the kurtosis parameter for simplicity and clarity. A particularly noteworthy result is shown in Fig. 8, which illustrates the spectral energy ratio between damaged and healthy signals for both sensors, calculated on the 1/3-octave spectrum. The results clearly indicate a gradual increase in the energy ratio with increasing shaft speed for both microphones. In particular, the measurement microphone shows an increase in spectral energy in the range from 6.3 to 16 kHz, peaking at 8 kHz. On the other hand, the ultrasonic microphone reveals two distinct regions of energy increase: one between 20 and 25 kHz and the other between 31.5 and 63 kHz. Interestingly, both microphones' effectiveness is significantly influenced by shaft speed, revealing weaker energy ratios at lower speeds. This tendency is more pronounced in the ultrasonic microphone but is also slightly evident in the measurement microphone. The accelerometer does not exhibit this velocity-dependent behavior, showing the highest energy ratio in the upper bands, particularly from 8 to 12.5 kHz. As might have been expected, in terms of amplitude of the spectral energy ratio, the accelerometer provides the most pronounced and reliable results.

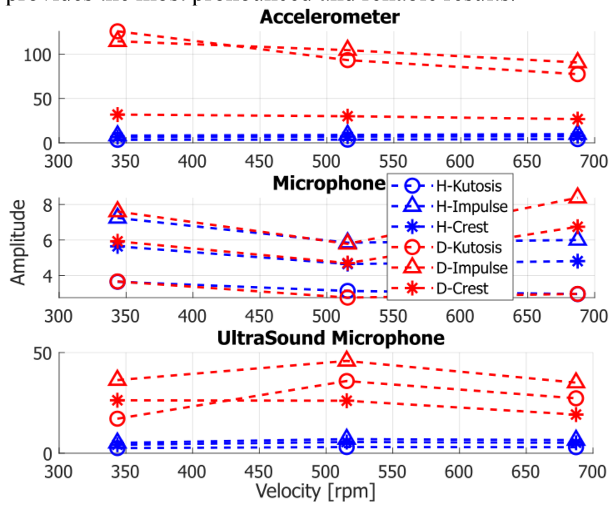

Figure 6. Statistical indicators at varying speeds.

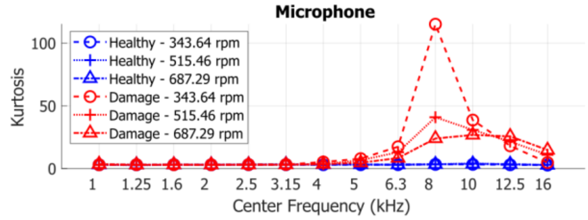

Figure 7. Microphone signal kurtosis in 1/3-octave bands.

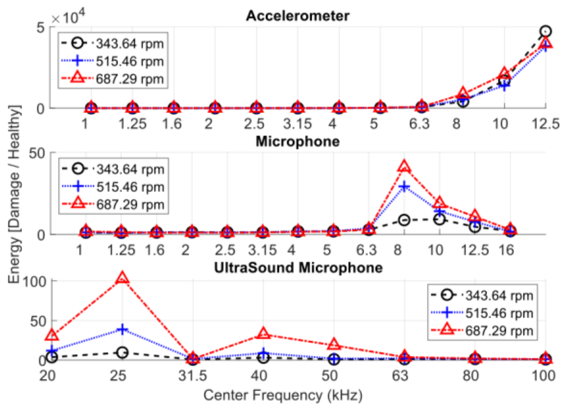

Figure 8. Energy Ratio between damaged and healthy bearings at varying speeds.

5. CONCLUSION

Microphones have proven to be a viable solution for detecting faults in rolling bearings under controlled conditions, offering a useful alternative in scenarios where accelerometers cannot be used. This study explored two basic data analysis techniques, both of which yielded promising results. In particular, the energy ratio method demonstrated strong potential for predictive maintenance applications, with performance comparable to that of traditional statistical indicators. While kurtosis can be an absolute indicator of failure, this is not necessarily true for the other statistical parameters or energy-based approaches. These methods were selected for their low computational cost and practical applicability in real-world predictive maintenance systems. The findings suggested that integrating ultrasonic microphones into vibroacoustic analysis frameworks can enhance the monitoring and maintenance of industrial systems. This approach was shown to be promising for improving the sensitivity of defect detection and providing, at the same time, practical benefits regarding ease of installation and maintenance.

6. FUTURE WORKS

This preliminary study applied classical statistical parameters and energy-based analysis techniques to signals acquired from accelerometric, acoustic, and ultrasonic measurements. Future work will explore advanced diagnostic signal processing methods and compare sensor performance under varying operating conditions, including changes in position and rotational speed. In particular, the influence of microphone distance will be investigated to simulate scenarios in which contact sensors, such as accelerometers, are not a feasible solution.

7. REFERENCES

[1] P. Nunes, J. Santos, and E. Rocha, "Challenges in predictive maintenance – A review," *CIRP J Manuf Sci Technol*, vol. 40, pp. 53–67, 2023.

[2] T. Zonta, C. A. da Costa, R. da Rosa Righi, M. J. de Lima, E. S. da Trindade, and G. P. Li, "Predictive maintenance in the Industry 4.0: A systematic literature review," Comput Ind Eng, vol. 150, p. 106889, 2020.

[3] M. Pech, J. Vrchota, and J. Bednář, "Predictive Maintenance and Intelligent Sensors in Smart Factory: Review," *Sensors*, vol. 21, no. 4, 2021.

[4] S. A. McInerny and Y. Dai, "Basic vibration signal processing for bearing fault detection," IEEE Transactions on Education, vol. 46, no. 1, pp. 149–156, 2003.

[5] J. Coady, D. Toal, T. Newe, and G. Dooly, "Remote acoustic analysis for tool condition monitoring," Procedia Manuf, vol. 38, pp. 840–847, 2019.

[6] A. Morhain and D. Mba, "Bearing defect diagnosis and acoustic emission," Proceedings of the Institution of Mechanical Engineers, Part J, vol. 217, no. 4, pp. 257–272, 2003.

[7] E. Y. Kim, A. C. C. Tan, J. Mathew, and B. S. Yang, "Condition monitoring of low speed bearings: A comparative study of the ultrasound technique versus vibration measurements," Australian Journal of Mechanical Engineering, vol. 5, no. 2, pp. 177–189, 2008.

[8] A. Rai and S. H. Upadhyay, "A review on signal processing techniques utilized in the fault diagnosis of rolling element bearings," Tribol Int, vol. 96, pp. 289–306, 2016.

[9] N. Rocchi, A. Toscani, G. Chiorboli, D. Pinardi, M. Binelli, and A. Farina, "Transducer Arrays over A^2B Networks in Industrial and Automotive Applications: Clock Propagation Measurements," *IEEE Access*, vol. 9, pp. 118232–118241, May 2021.

[10] A. Toscani, F. Immovilli, D. Pinardi, and L. Cattani, "A Novel Scalable Digital Data Acquisition System for Industrial Condition Monitoring," IEEE Transactions on Industrial Electronics, vol. 71, no. 7, pp. 7975–7985, Jul. 2024.

[11] N. Rocchi et al., "A Modular, Low Latency, A 2 B-based Architecture for Distributed Multichannel Full-Digital Audio Systems," in 2021 Immersive and 3D Audio: from Architecture to Automotive (I3DA), IEEE, Sep. 2021.

[12] D. Pinardi, L. Arpa, A. Toscani, E. Manconi, M. Binelli, and E. Mucchi, "A Novel Hybrid Acquisition System for Industrial Condition Monitoring and Predictive Maintenance," IEEE Access, vol. 12, pp. 98121–98129, 2024.

[13] R. B. Randall, Vibration-based condition monitoring: industrial, automotive and aerospace applications. John Wiley & Sons, 2021.